André Balogh · Leonid Ksanfomality ·
Rudolf von Steiger
Editors

# Mercury

Foreword by André Balogh, Leonid Ksanfomality and Rudolf von Steiger

Previously published in *Space Science Reviews* Volume 132, Issues 2–4, 2007

Springer

André Balogh
International Space Science
Institute (ISSI),
Bern, Switzerland

Rudolf von Steiger
International Space Science
Institute (ISSI),
Bern, Switzerland

Leonid Ksanfomality
Space Research Institute (IKI),
Moscow, Russia

*Cover illustration:* Three planets after sunset over Paranal Observatory, Chile. The lower planet is Mercury, the brightest at the centre is Venus, the one on the left is Saturn. Image courtesy and © Stéphane Guisard.



Library of Congress Control Number: 2008920289

ISBN-978-0-387-77538-8 e-ISBN-978-0-387-77539-5

Printed on acid-free paper.



1

springer.com

# Contents

# Introduction

**André Balogh · Leonid Ksanfomality · Rudolf von Steiger**

Originally published in the journal Space Science Reviews, Volume 132, Nos 2–4.
DOI: 10.1007/s11214-007-9293-0 

It is remarkable that Mercury, the messenger of the gods in ancient mythology, was discovered and identified in antique times. Unlike Venus and Mars, or even Jupiter and Saturn, Mercury is extremely difficult to observe by the unaided eye. It is, in fact, also very difficult to observe with astronomical telescopes, because of its proximity to the Sun and its small size. This means that, while Venus is a proud and very bright evening and morning "star", Mercury is, at its greatest visual elongation from the Sun, a very faint "twilight" or "daybreak" star. Despite that, the ancient Egyptian, Babylonian, Greek and other astronomers in the classical world recognised it as a wanderer against the starry background of the sky, noting its swift motion, and thus finding it an appropriate role in their mythology. For the Greeks, the god Hermes represented the planet and for the Romans, the god (and the planet) became Mercurius, now in English Mercury. Both appellations survive in planetary sciences: it is equally possible to speak of the Hermean magnetic field or the magnetic field of Mercury.

While there are fleets of increasingly sophisticated spacecraft targeting Mars—and Venus, Jupiter and Saturn remain of continuing interest to planetary scientists and space agencies—Mercury has suffered from being very difficult to reach and very difficult to observe from Earth. However, since the visits of the pioneering Mariner 10 spacecraft, there has been a steady effort to achieve a better understanding of Mercury. This has been done (a) by a sustained programme of ground-based observations by a dedicated set of planetary scientists, (b) by very fully exploiting the so-far unique Mariner 10 archive of observations

A. Balogh (✉)
International Space Science Institute (ISSI), Hallerstrasse 6, Bern 3012, Switzerland
e-mail: balogh@issibern.ch

L. Ksanfomality
Space Research Institute, Russian Academy of Sciences, Profsoyuznaya St. 84/32,
Moscow 117810, Russia

R. von Steiger
International Space Science Institute (ISSI), Hallerstrasse 6 Bern 3012, Switzerland

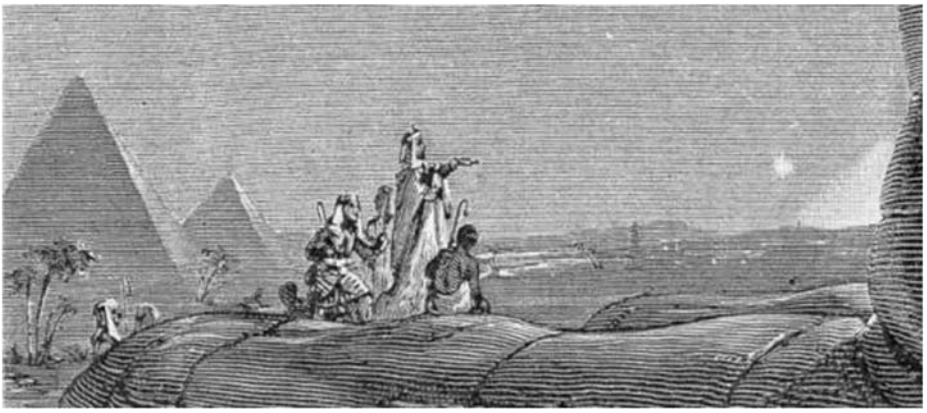

A nineteenth century illustration imagining the ancient Egyptians admiring Mercury at sunset. (After an engraving of Régnier Barbant in G. Flammarion, *Astronomie Populaire*, 1881, discovered by Réjean Grard during the long, drawn-out study phase of what became the BepiColombo mission)

and (c) by theoretical and modelling research to understand the evolution and current state of the planet and its known peculiarities, in particular its high density and its planetary magnetic field. It is generally recognized that understanding Mercury is one of the keys to understanding the origin and formation of the solar system.

The Workshop on Mercury held at the International Space Science Institute in Bern, on June 26–30, 2006, gathered a group of scientists who have dedicated a significant part of their career to this planet. The main objective was to review the achievements of the past 30 years and more in Mercury research, at the dawn of a new phase for the scientific investigations of Mercury by the forthcoming MESSENGER and BepiColombo missions. This volume is the result of the collaborations established at the Workshop.

The images taken by Mariner 10 almost 35 year ago have been extensively studied, although even now new and innovative image processing (not available to the first researchers after Mariner 10) have yielded new understanding of the surface features, as summarised by Gabriele Gremonese and his co-workers in this volume. However, in the absence of new space-based observations since Mariner 10, there have been remarkable achievements by ground-based observers. The continuously improved radar imaging of Mercury, particularly by the Goldstone radar and most importantly by the Arecibo giant dish (as described in this volume by John Harmon) has produced a range of observations which have provided major discoveries. Most prominent among these is the identification of radar-bright deposits in (mostly) near polar craters, indicating the possible presence of water ice where permanent shadowing by the crater walls may have preserved accumulated ice deposits over time. Further evidence for that is that the lesser shading of mid-latitude craters provides radar images of deposits in the expected shaded portion of such craters. In addition to this discovery, radar images of remarkable resolution and clarity have been obtained on the hemisphere not imaged by Mariner 10. A new light has also been shed on several surface features that had been imaged by Mariner 10. Our knowledge of Mercury has greatly benefited from the radar observations; it is likely that further radar observations may again be used as complementary information when the new missions, MESSENGER in the first place, will provide images of the so-far unseen side of Mercury.

Visual observations of Mercury from the ground are very difficult. Evidence for that comes from observations and drawings made by prominent planetary astronomers before

the Mariner 10 mission that were found to be largely unrepresentative of the real surface features. New technologies in imaging and image processing have overcome some of those early difficulties. Interestingly, the ground-based visual observations have brought additional information on aspects of the nominally much higher resolution observations by Mariner 10 and also, of course, on intriguing features on Mercury's so-far unknown hemisphere as described by Leonid Ksanfomality and his co-authors in this volume. It seems that it will be impossible to better the ground-based images reported on in that paper, but experience shows that ground-based images may well remain useful in the future.

The composition and texture of Mercury's surface are important unknowns in efforts to determine the history and evolution of the planet. Spectral imaging of Mercury at visible and near-infrared wavelengths from Earth faces, of course, the same technical problems and may be even more difficult than the imaging of the visible features. Nevertheless, as reported by Ann Sprague and co-workers in this volume, notable progress has been made in multispectral imaging and in the analysis, interpretation and modelling of the observations. Both known and unknown hemispheres seem to show the silicate-dominated, heavily cratered surface characteristics, with a probably very important part influenced in its details by space-weathering, that is the direct impact of particulate matter as well as atomic particles in the solar wind and cosmic rays.

Moving away from the surface, Mercury has no atmosphere but only a tenuous, almost certainly highly variable exosphere. While the expected atomic hydrogen, helium and atomic oxygen components were observed from close-by during the Mariner 10 flybys of Mercury, the quantitative results have remained in some doubt and will be clarified with the arrival of the orbiters around the planet. As recounted in detail by Rosemary Killen and her co-authors (this volume), real progress has been made in the past 15 to 20 years from the observation of sodium and potassium emission lines observed from the ground. Although the spatial resolution of the observations is rather coarse when compared to even the visible or near-infrared observations from Earth, the Na lines have shown a remarkable variability in intensity and in location. There are strong presumptions that the emissions are modulated by activity in the magnetosphere of Mercury. Stefano Orsini and co-workers in this volume explore the connections in the obviously complex and time variable surface–exosphere–magnetosphere system.

Mercury's magnetosphere remains a fascinating subject and it is very important that new observations from the forthcoming orbiters extend very significantly the seemingly very small, yet highly productive data archive from two flybys of Mariner 10. In all, the total amount of data corresponds to about 45 minutes from the first and third Mariner 10 flybys. Although no new data can be obtained without visiting Mercury again, the data we possess have been subjected to many imaginative interpretations. On the one hand, there is an Earth-like aspect, but with the planet filling a much greater proportion of the volume of the magnetosphere than is the case at the Earth. On the other hand, the small planetary magnetic field, the higher variability (in absolute terms) of the dynamic effects of the solar wind produce very short time and spatial scales for magnetospheric phenomena than those with which we are familiar at Earth. The absence of an ionosphere is a major difference between Mercury and Earth, and the role played by the surface and exosphere in closing current systems remains unknown. Reviews in this volume by Matsumi Fujimoto, Lev Zelenyi, Lars Blomberg and their respective co-authors provide a good progress report of the numerous analyses and interpretations of the Mariner 10 data.

Although Mercury's comparatively high density was known before Mariner 10—implying a large, iron-dominated core—the discovery of the planetary scale magnetic field was completely unexpected. This discovery justified totally the inclusion of a magnetometer in the space probe's payload despite expert opinion that insisted on the frozen state of

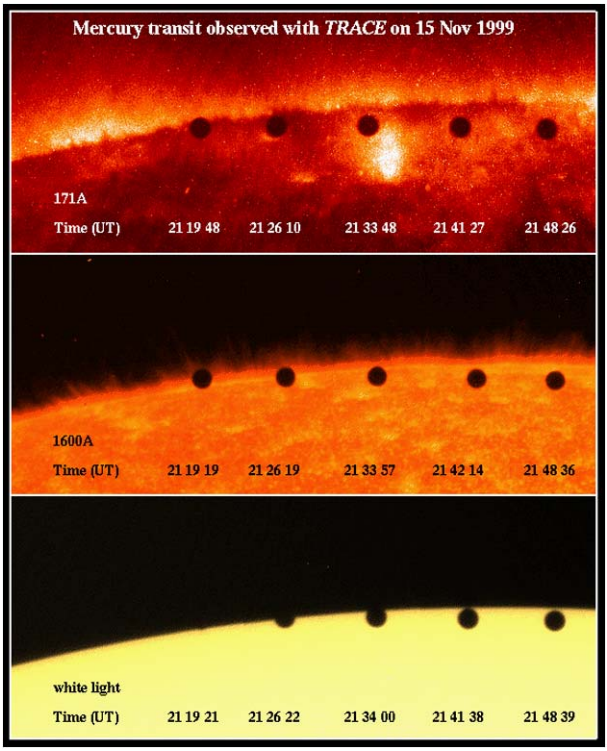


A time-elapsed series of the Mercury transit across the solar disk on November 15, 1999, observed by the TRACE spacecraft in three wavelengths, corresponding to (from top to bottom) the hot lower corona, the chromosphere and the photosphere. The transit is a very good illustration of the difference in scales between the Sun and the planet. Observations of Mercury transit have historically helped with the timing of Mercury's orbit and also to discover general relativity effects in its orbital period. (With acknowledgement to the TRACE team, Lockheed Martin Solar and Astrophysics Laboratory.)

Mercury's core and therefore the certain absence of a planetary dynamo. Clearly, we need considerably more data on the planetary magnetic field that can only come from the orbiters. Yet the simple existence and small magnitude of the magnetic field has continued to provide very big challenges to understanding the evolution and the current state of Mercury's interior, and constructing a planetary dynamo based on the interior modelling. The qualitative and quantitative constraints on the interior and the best current theories and models of the evolution and interior structure are reviewed in this volume by Tim van Hoolst and Doris Breuer and their respective co-authors. The increasingly sophisticated considerations that have become necessary to account for the relatively simple factual observations of the density and the magnetic field have now yielded an understanding that could be, but perhaps will not be challenged, although certainly refined by the observations to come.

Identifying the origin of the magnetic field remains a source of considerable difficulty. Not only is the internal structure of Mercury challenged by the existence of a planetary scale magnetic field, but what we know of the formation and functioning of planetary dynamos in general. The Mariner 10 data set is simply not sufficient to characterise and constrain an internal dynamo, or possible alternative sources in any detail. Nevertheless, over the past few years many of the conceptual and modelling difficulties have been thoroughly researched and many of those clarified. The status of our understanding of Mercury's internal magnetic field, including the very latest and significant developments, are described by Johannes Wicht and his co-authors in this volume. On this topic, perhaps more than any other related to Mercury, the new observations to come from the forthcoming orbiters are absolutely vital. Magnetic field measurements may well provide the most important information on the planet's interior as well as its environment. Therein lies a significant difficulty. The mag-

netic field that will be measured by the orbiters is a complex, nonlinearly interacting sum of the field internal to the planet and that generated by the highly variable currents due to the interaction of the solar wind with the planetary magnetic field. One representative aspect of this interplay between internal and external effects is the component of the magnetic field due to the induction field in the conductive core generated by external currents, as discussed in this volume by Karl-Heinz Glassmeier and his co-authors. Estimates of the contributions by the internal and external sources show that at any time and any place in the orbit around Mercury the contributions are likely to be of comparable magnitude, yet also variable, thus making the careful measurement and analysis of the magnetic field one of the most important objectives of the two orbiter missions.

There have been many proposals since Mariner 10 for the necessary space missions to Mercury, as described in this volume by André Balogh and his co-authors. It is quite remarkable that, after a lull of 35 years, two major space probes are targeting the planet Mercury. The first of these, NASA's MESSENGER, will make a first flyby of the planet in January 2008, before another flyby in 2008, then one in 2009, before finally inserted into orbit around Mercury in 2011. The joint, more ambitious, two-spacecraft BepiColombo mission by the European Space Agency and Japan's Institute of Space and Astronautical Sciences (a part of JAXA) will be launched in 2013 and will reach Mercury orbit in 2019. These two space missions will satisfy the lively curiosity of the two generations of planetary scientists who have worked, since the pioneering days of NASA's Mariner 10 mission in 1974–1975, on discovering the properties and peculiarities of this, the closest planet to the Sun and at least a distant cousin of the Earth in the family of terrestrial planets.

There is, however, a fundamental question that may not be answered, at least not simply or directly so, by the forthcoming space missions. That question is the origin of Mercury. As a member of the family of the four terrestrial planets (and the Moon), the formation of Mercury is an important aspect of our understanding of the terrestrial planets, their origin, formation and evolution. Willy Benz and his co-authors revisit, in this volume, this fundamental question and set out the likely scenarios that lead to the planet Mercury as we know it, in the orbit that we also know. It seems quite likely that neither planet nor its orbit is "original". This question is expected to remain on the agenda for the future, not least in an era when planetary systems around other stars increasingly become objects of close scrutiny.

The Editors are very happy to thank all those who have contributed to this volume and to the workshop. First of all, we thank the authors for their integrated approach to distil the presentations and discussions in the Workshop, in particular those who accepted the responsibility to coordinate the articles in this volume. All the papers were peer reviewed by referees, and we thank the reviewers for their helpful and critical reports. We also thank the directorate of ISSI for selecting Mercury as the topic for the workshop, and the advice of ISSI's Science Committee on this subject. We thank the staff of ISSI, in particular Roger Bonnet for his support of the workshop, and also Brigitte Fasler, Andrea Fischer, Vittorio Manno, Saliba F. Saliba, Irmela Schweizer and Silvia Wenger for their help, patience and good humour to provide a productive environment for the workshop.

# The Origin of Mercury

**W. Benz · A. Anic · J. Horner · J.A. Whitby**

Originally published in the journal Space Science Reviews, Volume 132, Nos 2–4.
DOI: 10.1007/s11214-007-9284-1 

**Abstract** Mercury's unusually high mean density has always been attributed to special circumstances that occurred during the formation of the planet or shortly thereafter, and due to the planet's close proximity to the Sun. The nature of these special circumstances is still being debated and several scenarios, all proposed more than 20 years ago, have been suggested. In all scenarios, the high mean density is the result of severe fractionation occurring between silicates and iron. It is the origin of this fractionation that is at the centre of the debate: is it due to differences in condensation temperature and/or in material characteristics (e.g. density, strength)? Is it because of mantle evaporation due to the close proximity to the Sun? Or is it due to the blasting off of the mantle during a giant impact?

In this paper we investigate, in some detail, the fractionation induced by a giant impact on a proto-Mercury having roughly chondritic elemental abundances. We have extended the previous work on this hypothesis in two significant directions. First, we have considerably increased the resolution of the simulation of the collision itself. Second, we have addressed the fate of the ejecta following the impact by computing the expected reaccretion timescale and comparing it to the removal timescale from gravitational interactions with other planets (essentially Venus) and the Poynting–Robertson effect. To compute the latter, we have determined the expected size distribution of the condensates formed during the cooling of the expanding vapor cloud generated by the impact.

We find that, even though some ejected material will be reaccreted, the removal of the mantle of proto-Mercury following a giant impact can indeed lead to the required long-term fractionation between silicates and iron and therefore account for the anomalously high mean density of the planet. Detailed coupled dynamical–chemical modeling of this formation mechanism should be carried out in such a way as to allow explicit testing of the giant impact hypothesis by forthcoming space missions (e.g. MESSENGER and BepiColombo).

**Keywords** Mercury: origin · Planets: formation · Numerics: simulation

W. Benz (✉) · A. Anic · J. Horner · J.A. Whitby
Physikalisches Institut, University of Bern, Sidlerstrasse 5, 3012 Bern, Switzerland
e-mail: wbenz@space.unibe.ch

J. Horner
Astronomy Group, The Open University, Walton Hall, Milton Keynes MK7 6AA, UK

A. Balogh et al. (eds.), *Mercury*. DOI: 10.1007/978-0-387-77539-5_2 

## 1 Introduction

The density of Mercury, mean density 5.43 g/cm$^3$ (Anderson et al. 1987), uncompressed mean density ∼5.3 g/cm$^3$ (Cameron et al. 1988), is anomalously high. For comparison we note that the uncompressed mean density of the Earth is just ∼4.45 g/cm$^3$ (Lewis 1972). From this Urey (1951, 1952) noted that Mercury must have an iron-to-silicate ratio much larger than that of any other terrestrial planet. The silicate-to-iron mass ratio is usually estimated to lie in the range from 30 : 70 to 34 : 66 or roughly 0.5. Harder and Schubert (2001) argued that the presence of sulfur in the core could lead to even smaller ratios and that a planet entirely made of FeS could not be excluded. All of these ratios are many times smaller than those of any of the other terrestrial planets or the Moon.

A variety of hypotheses have been suggested to account for the anomalously high mean density of Mercury. In all cases, the close proximity of Mercury to the Sun plays a crucial role and all theories invoke processes that result in some level of fractionation between iron and silicates during the very early phases of the solar system in order to explain this strange mean density. Amazingly, all these scenarios and ideas date back some 20 years or more. As far as the origin of the planet is concerned, very little new work has been carried out during the last two decades. In our opinion, this reflects more the lack of new relevant data than a lack of interest in the origin of this end member of the solar system. Although new ground-based observations of Mercury have been made since the Mariner 10 mission (Sprague et al. 2007), these have not yielded a consensus on the detailed geochemical and geophysical parameters necessary to distinguish between models of Mercury's formation. It is clear that with the two new space missions dedicated to study Mercury in unprecedented detail (NASA's MESSENGER and ESA's BepiColombo; see e.g. Balogh et al. (2007)), this situation is about to change drastically. It is therefore critical to revisit the problem of the origin of Mercury and to work out models that make testable predictions in order to prepare the necessary framework in which to discuss the measurements the two future missions will be able to carry out.

Mercury formation models which have been proposed to account for this anomaly can be classified into two broad categories according to the time at which the fractionation occurs. In the first category, we find models that explain the anomalous composition of the planet as a result of fractionation that occurred during the formation of the planet proper. The second set of models encompasses those for which the planet forms first with roughly chondritic abundances and fractionates shortly thereafter. We shall briefly review these two categories in Sect. 2.

Studying Mercury's origin involves studying the dynamics and chemistry of the protoplanetary nebula in close proximity to the star. Since planets grow through collisions, the study of the formation of Mercury is also an investigation of these processes in a region where these collisions are particularly violent. Although the details of the study may be specific to just this planet, it holds implications for the formation of rocky planets (or the cores of giant planets) in general, and may provide a means for choosing between different theories.

## 2 The Formation of Mercury: Scenarios and Ideas

In this section we briefly recall the different scenarios that have been proposed to explain Mercury's anomalous composition. In all the currently available scenarios, the main point is to achieve enough chemical fractionation to account for the high density of the planet. Not

surprisingly, all these scenarios take place very early on in the history of the solar system either as an ongoing process during the formation of the planets, or during the late stages of accretion or shortly thereafter. They all rely in some way on the peculiar position of the planet, namely its close proximity to the Sun.

## 2.1 Fractionation During Formation

In this class of models, the anomalous density of Mercury results from fractionation occurring during the formation process itself. In its simplest form, fractionation is obtained as a result of an equilibrium condensation process in a proto-planetary nebula in which the temperature is a monotonic function of the distance to the Sun (Lewis 1972, 1974; Barshay and Lewis 1976; Fegley and Lewis 1980). Such models predict that the condensates formed at Mercury's distance were both extremely chemically reduced and extremely poor in volatiles and FeO. Metallic iron would be partially condensed while refractory minerals rich in calcium, aluminum, titanium and rare earths would be fully condensed. The bulk average density of the condensed material would therefore be much higher in the Mercury region than in the formation regions of the other terrestrial planets hence explaining the high mean density.

Although such simple models of the chemical behavior of the solid material in the early solar nebula successfully predict some of the most general compositional trends of solar system bodies, it was recognized by Goettel and Barshay (1978) and later by Lewis (1988), that this mechanism cannot explain the anomalous density of Mercury. The main reason for the failure of this model is the relatively small difference in the condensation temperature of core and mantle material. This implies also a close spatial proximity in the nebula while the area over which the material must be collected to actually bring a planetary mass together, is much larger. The high-density material is simply diluted with lower density material. Lewis (1988, and references therein) showed that this results in a maximum core mass fraction of about 36% as compared to the 70% for the actual planet. Hence, simple condensation–accretion models fail to explain the mean density of Mercury.

To circumvent these difficulties, various additional fractionation mechanisms operating during, or even before, the start of planetary accretion have been proposed. While some combination of these mechanisms based on microscopic differences between silicates and iron (ferromagnetism, strength, etc.) may possibly lead to higher mean densities, there exist no compelling reasons why these mechanisms should have been more active at Mercury than other places in the solar system (see Weidenschilling 1978 for a detailed discussion). Weidenschilling (1978), on the other hand, proposed that the additional fractionation results from a combination of gravitational and drag forces. As the early condensates orbited the Sun, immersed in a gaseous disk, they felt a drag force that depends in a complex fashion upon the size and shape of the condensed particles and upon the structure of the nebula. As a result of this drag force, orbiting bodies lose angular momentum and spiral inward. In a simple quantitative model, Weidenschilling (1978) showed that the rate of orbital decay is slower for larger and/or denser bodies. With suitable but reasonable assumptions for the initial conditions, Weidenschilling (1978) showed that the fractionation required to produce iron-rich planets can be achieved.

Following the three-dimensional dynamics of a dusty gas over periods of time vastly exceeding a dynamical timescale is a complicated problem, especially since the dynamics of the gas itself is still up for debate. For example, the origin of the turbulence, the existence of instabilities, the presence of spiral waves, among others, are still unclear. Hence, short of a better understanding of the dynamics of this multicomponent fluid, it is difficult to assess to

what extent models based on fractionation occurring in a laminar nebula before and during planet formation are realistic.

### 2.2 Fractionation after Formation

Cameron (1985) proposed that, during the early evolution of the solar nebula, temperatures at the position of Mercury were probably in the range 2,500–3,000 K. If a proto-Mercury existed at the time, partial volatilization of the mantle would occur thus creating a heavy silicate atmosphere which could over time be removed by a strong solar wind. Fegley and Cameron (1987) computed the expected bulk chemical composition of the mantle as a function of evaporated fraction using both ideal and nonideal magma chemistry. They showed that starting with a proto-Mercury of chondritic abundance (2.25 times the mass of the present day planet) Mercury's mean density can be obtained after 70–80% of the mantle has evaporated. At this point, the remaining mantle is depleted in the alkalis, FeO and $SiO_2$, but enriched in CaO, MgO, $Al_2O_3$ and $TiO_2$ relative to chondritic material. Fegley and Cameron (1987) argued that this anomalous composition represents a unique signature of this formation scenario that could eventually be measured by a dedicated spacecraft mission.

This scenario has the clear advantage of having its consequences calculated in enough detail to allow potentially explicit testing. However, it also suffers from a number of difficulties. For example, it is not clear whether high enough temperatures can be reached and maintained for long enough in the solar nebula *after* a suitable proto-Mercury has been formed. Furthermore, as already identified by Cameron (1985) himself, the solar wind may not be efficient enough to remove the heavy silicate atmosphere thus preventing a significant evaporation of the mantle.

In another scenario to explain Mercury's anomalous density, the removal of a large fraction of the silicate mantle from the originally more massive proto-Mercury is achieved following one (or possibly more) giant impacts (Smith 1979; Benz et al. 1988; Cameron et al. 1988). In this hypothesis, a roughly chondritic Mercury (2.25 times the mass of present day Mercury) is hit by a sizable projectile (about 1/6 its mass in the calculations by Benz et al. 1988) at relatively high velocity. Such an impact results in the loss of a large fraction of the mantle leaving behind essentially a bare iron core (see Sect. 3). The existence of large projectiles was first suggested by Wetherill (1986), who realized that terrestrial proto-planets probably suffered collisions with bodies of comparable mass during the final stages of their formation. He also proposed that the high relative velocities in Mercury's formation region could lead to particularly disruptive collisions making the formation of Mercury unique among the terrestrial planets.

Simulations (Benz et al. 1988; Cameron et al. 1988) have shown that the required removal of the silicate mantle can be achieved by a giant impact. However, the question of the long-term fate of the material ejected from such an impact has never been properly investigated. Indeed, most of the ejected material following the impact is still orbiting the Sun on Mercury crossing orbits and will therefore eventually collide with the planet and be reaccreted over time unless it is removed by some other processes. If a significant fraction should indeed be reaccreted, the fractionation obtained as a result of the collision would only be short lived and therefore would not explain the present-day mean density of the planet.

Both gravitational scattering and the Poynting–Robertson effect have been invoked as possible ejecta-removal mechanisms. However, the former is found to remove only a very small amount of material (see Sect. 4.1) and the efficiency of the second depends on the size distribution of the ejecta. Simple condensation models based on equilibrium thermodynamics (Anic 2006) show that the expanding vapour cloud following the impact would

lead to the formation of small-sized condensates (see Sect. 4.1). These small-sized condensates can readily be affected by nongravitational forces such as those originating from the Poynting–Robertson effect. Hence, from a dynamical point of view, the giant impact scenario as proposed by Benz et al. (1988) and Cameron et al. (1988) appears to be possible. It remains to be determined, however, whether the chemical signature of such a giant impact is compatible with the bulk chemistry of Mercury.

## 3 Simulations of Giant Impacts

### 3.1 Initial Conditions

As the target body in our collision simulations, we adopt a proto-Mercury that has roughly chondritic abundance. We built such a proto-Mercury by increasing the mass of the silicate mantle of the planet until the present-day core mass represents only about 1/3 of the planet's total mass. With this structure, the total mass of proto-Mercury amounts to 2.25 times the mass of present-day Mercury. Its internal structure is computed using the usual equations assuming an adiabatic temperature profile (Spohn et al. 2001). For the equation of state (EOS) in our calculations we use ANEOS (Thompson and Lauson 1984). This analytical EOS relates temperature and density to pressure, and describes mixed states (liquid–vapour, solid–vapour) using the Helmholtz free energy potential. The equation requires 24 coefficients for a given material which, for the most part, can be derived from laboratory experiments. We assume that the mantles of the projectile and the target consist of dunite (a rock consisting largely of forsteritic olivine $Mg_2SiO_4$) which has similar bulk properties to mantle rock. The table of parameters for dunite was given by Benz et al. (1989). The core of the planet is assumed to consist of pure iron.

Finally, we must specify boundary conditions and in particular the value of the temperature at the surface of the planet and the projectile. Since this value is not known at the time of formation of the planet, we use two different values which should bracket the possibilities reasonably well. In one case, we use the present-day mean surface temperature of 452 K and for the other we consider a much hotter body with a surface temperature of 2,000 K. We shall refer to these two models in the text as *cold* and *hot*.

### 3.2 Numerics and Model Assumptions

Following Benz et al. (1988), we use a 3D Smooth Particle Hydrodynamics (SPH) code to simulate the impacts. SPH is a Lagrangian method in which the motion of the mass elements (particles) is followed over time. Given that SPH has already been described many times in the literature and that we use a fairly standard implementation of the method, we refer the reader to reviews by Benz (1990) and Monaghan (1992) for further detailed explanation of the method. In the present work, we use the version of SPH described by Benz (1990), with only a small number of modifications. The major change is the use of individual artificial viscosity coefficients that vary over time using the shock detection algorithm proposed by Morris and Monaghan (1997), which minimises the viscosity outside shocks.

In all cases, we neglected the strength of the material. This assumption is reasonable given the size of the bodies involved for which self-gravity and pressure gradients are the dominating forces. Self-gravity is computed using a hierarchical binary tree as discussed by Benz (1990). We also neglect radiative losses during the impact (cooling due to adiabatic

expansion is included). The main reason for this is to avoid the considerable additional numerical work that would be needed to compute such radiative losses. From a physical point of view, the assumption is justified by the fact that the simulations proper extend only over a relatively short amount of real time during which the radiative losses should remain small. We investigated simple models of radiative cooling as part of the condensation calculations presented in Sect. 4.1.

The simulations were carried out until the ultimate fate of the material could be reliably determined. At that time, we identified the material having being lost by the planet using the same iterative procedure (based on binding energy) as described by Michel et al. (2002). For the material remaining gravitationally bound, we compute the fractions of silicate and iron in order to determine the rock-to-iron (R/I) ratio.

### 3.3 Results

We performed a number of simulations of giant collisions with different projectile masses, impact velocity and impact geometries in order to find collisions that lead to a suitable fractionation. However, we did not carry out an extensive search to find all the possible initial conditions leading to the desired result. Hence, we cannot compute the actual probability of such an event. However, we note that success (see Table 1) does not involve exceptional geometries or mass ratios. On the other hand, the velocity at which the two large bodies must collide in order to ensure almost complete mantle loss is relatively high. Such high relative velocities are much more likely to occur in the inner regions of the solar system

**Table 1** Simulations involving the "cold" (runs 1–12) and "hot" (runs 13–17) proto-Mercury

| Run | $b$ [R] | $v_{\rm rel}$ [km/s] | $m_{\rm imp}/m_{\rm tar}$ | $N_{\rm p}$ | $N_{\rm t}$ | $R/I$ | $M_f$ |
|---|---|---|---|---|---|---|---|
| 1 | 0.7 | 30 | 0.1 | 11′326 | 113′129 | 1.32 | 1.73 |
| 2 | 0.5 | 27 | 0.1 | 15′543 | 155′527 | 1.10 | 1.50 |
| 3 | 0 | 20 | 0.1 | 11′326 | 113′129 | 1.25 | 1.63 |
| 4 | 0.5 | 26 | 0.167 | 23′556 | 141′392 | 0.78 | 1.18 |
| 5 | 0.53 | 28 | 0.167 | 23′556 | 141′392 | 0.59 | 1.01 |
| 6 | 0 | 20 | 0.167 | 23′556 | 141′392 | 0.61 | 0.92 |
| 7 | 0 | 26 | 0.167 | 23′556 | 141′392 | 0.11 | 0.15 |
| 8 | 0.7 | 26 | 0.2 | 49′485 | 247′423 | 1.11 | 1.52 |
| 9 | 0.7 | 28 | 0.2 | 28′269 | 141′392 | 0.94 | 1.38 |
| 10 | 0.6 | 30 | 0.2 | 27′411 | 137′200 | 0.51 | 0.94 |
| 11 | 0.5 | 28 | 0.2 | 27′411 | 137′200 | 0.50 | 0.86 |
| 12 | 0 | 28 | 0.2 | 27′411 | 137′200 | – | 0 |
| 13 | 0.47 | 23 | 0.167 | 21′205 | 127′249 | 0.87 | 1.27 |
| 14 | 0.5 | 24 | 0.167 | 21′205 | 127′249 | 0.86 | 1.26 |
| 15 | 0 | 19 | 0.2 | 28′269 | 141′392 | 0.71 | 1.01 |
| 16 | 0.46 | 25.5 | 0.2 | 28′269 | 141′392 | 0.51 | 0.87 |
| 17 | 0.5 | 28 | 0.2 | 28′269 | 141′392 | 0.49 | 0.85 |

$N_{\rm p}$ is the number of particles in the projectile and $N_{\rm t}$ in the target. The impact parameter $b$ is given in units of target radius and the relative velocity is given in km/s. $R/I$ is the silicate to iron ratio in the surviving planet and $M_f$ is its final mass in units of present-day Mercury mass. The planet in run 12 disintegrated

where the Keplerian velocities are already large. Hence, extreme collisional fractionation of full-grown planets can, from a theoretical point of view, involve only planets orbiting deep in the potential well. This is consistent with the fact that Mercury is the only planet in the solar system with such a high mean density.

The initial conditions for the simulations performed and the final characteristics of the surviving planets are given in Table 1. Note that some of the runs are very similar to those performed by Benz et al. (1988) but with a considerable increase in the number of particles used (typically 20 to 50 times more).

In the various cases listed in this table, the collisions leading to a final mass of $M_f \approx 1$ (in units of present day Mercury mass) and a silicate to iron mass ratio $R/I = 0.4$–$0.6$ can be considered as successful in the sense that they reproduce the bulk characteristics of present-day Mercury. In fact, depending upon the subsequent reaccretion of a fraction of the silicate mantle (see Sect. 4), simulations with $R/I$ less than the present-day value should be considered as successful.

Note that, in order to remove a sizable fraction of the silicate mantle, the collision speed must be quite high, especially in the case of an off-axis collision for which the strength of the shock is significantly weaker (all other parameters being equal). Statistically, the most probable collisions are those with $b = 0.7 R_{\text{proto-Mercury}}$ (Shoemaker 1962) where the impact parameter $b$ is defined as the distance from the centre of the target to the centre of the impactor along a line normal to their relative velocity ($b$ is thus zero for a head-on collision and $R_{\text{proto-Mercury}} + R_{\text{impactor}}$ for a grazing collision). However, for realistic relative velocities and reasonable-sized projectiles, these dynamically most probable collisions seem not to result in a large enough loss of mantle material.

Overall, the simulations that appear to yield potentially satisfactory results are runs 6, 10, 11 in the case of a "cold" proto-Mercury and runs 16, 17 for the "hot" progenitor. Hence, as far as the initial blasting off of the mantle is considered, the thermal state of the progenitor does not appear to play a major role. Collisions involving "hot" bodies are not overwhelmingly more disruptive that those involving "cold" ones. In fact, similar results can be obtained by relatively small changes in collision characteristics. To illustrate a typical collision, Fig. 1 shows a set of four snapshots illustrating run 11.

We note how severe this collision actually is. The planet is nearly destroyed in the process and it is actually gravitational reaccumulation that brings the core of the planet back together. Such nearly destructive collisions are required if most of the mantle of a roughly chondritic proto-Mercury is to be removed. This also shows that destroying *large* bodies by means of collisions is not so easy and requires large impactors and high velocities. We argue that this implies that such events can only occur in regions near the star where the collision velocities can be high enough. If this is correct, it could explain why only Mercury fractionated to such an extent even though all the other terrestrial planets also experienced giant collisions during their formation. This makes Mercury particularly important for the study of terrestrial planet formation. We also note that as a result of the severity of the impact, all the material reaches high temperatures and thus the assumption made by Harder and Schubert (2001), that a Mercury formed by means of a giant impact could have a volatile rich composition and lose more iron than sulfur during the collision, seems unlikely to be true.

Finally, we point out that our run 5 had almost identical initial conditions to run 13 by Benz et al. (1988) and that the outcomes are very similar even though in this work we have been able to use about 50 times as many particles!

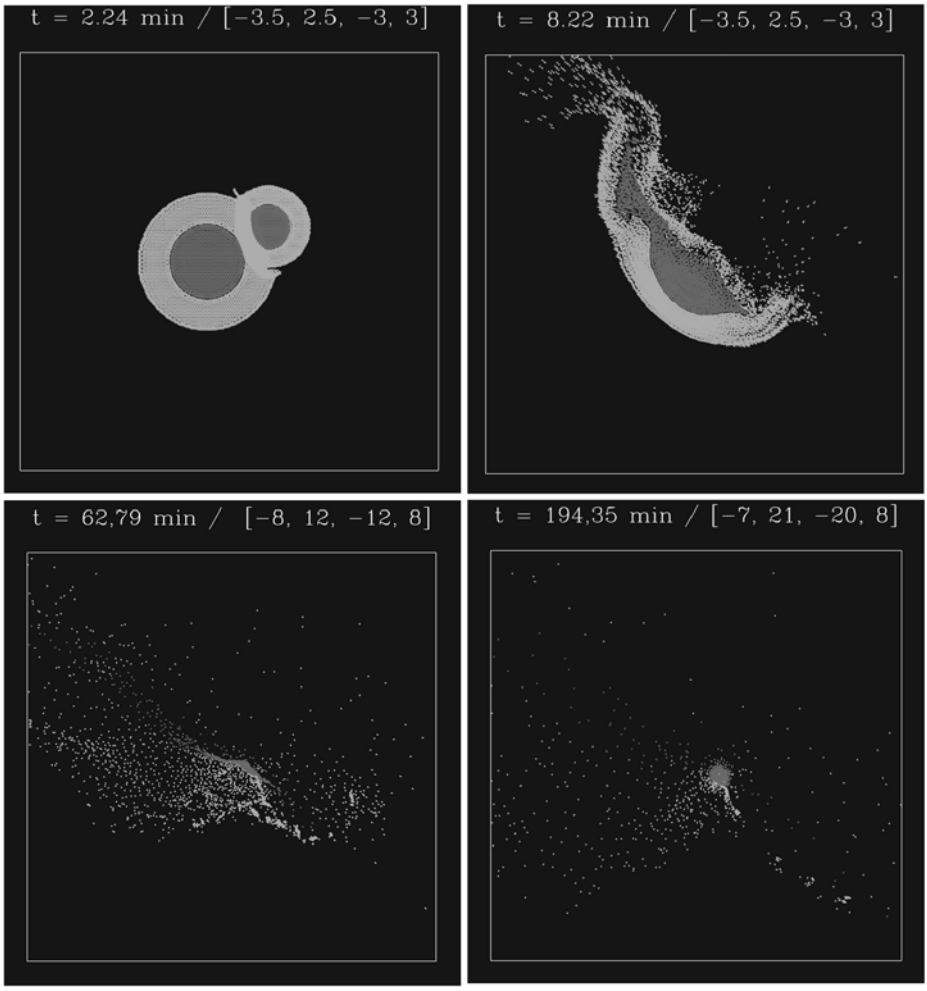


**Fig. 1** Snapshots from the evolution of run 11. Particles in a slice running through the central plane are plotted. Velocity vectors are normalized to the maximum vector in each figure and plotted at particle locations. Iron is shown in *dark grey*, whilst *light grey* represents silicates. The time after first contact (in minutes), along with the coordinates of the quadrant given in units of target radius, is given above each snapshot

## 4 The Fate of the Ejecta

As mentioned in Sect. 1, a giant impact removes most of the rocky mantle is not sufficient to explain the present-day bulk composition of Mercury. It is also necessary to demonstrate that the overwhelming part of the ejected matter is not reaccreted by the planet over time. For this to happen, it needs to be removed from Mercury crossing orbits before it collides with the planet again. In order to address these issues, we first computed the size distribution of the ejected matter (Sect. 4.1) and then compared the timescale required by the Poynting–Robertson effect to remove the ejecta (Sect. 4.2) with the timescale until collision with the planet (Sect. 4.3). We also investigated how effective gravitational torques exerted by other planets can be in ejecting the material (Sect. 4.3).

### 4.1 Size Distribution of the Ejecta

To compute the final size distribution of the ejected matter it is necessary to follow its thermodynamical evolution. This is conveniently done by using a $T-\rho$ diagram such as that sketched in Fig. 2. In our calculations we assume equilibrium thermodynamics, neglecting all rate-dependent effects. To check the importance of the equation of state, we computed the cooling curves using both a perfect gas EOS and ANEOS. For simplicity, but partially justified by the short duration of the impact, we also omit radiative losses and assume that the internal energy of the hot gas is entirely transformed into the kinetic energy of the expansion. Finally, in following the ejected matter, we treat each SPH particle as an independent piece of material ignoring the potential interactions (heat exchange, collisions, etc.) between the expanding particles. The overall size distribution is obtained by summing up the distributions obtained for all ejected SPH particles.

Upon being struck by a very large, fast-moving body, a large fraction of the target material is compressed to extreme pressures at which both metallic and siliceous liquids exhibit characteristics of a supercritical fluid ("hot vapour" in what follows). The path followed by the material during this compression phase is shown by ① in Fig. 2. During the subsequent very rapid decompression of the compressed liquid and the expansion of the hot vapour the matter undergoes a phase transition from either the liquid or the vapour side of the vapour-liquid dome (respectively ② and ③ in Fig. 2). Depending upon the cooling path taken by the hot vapour, we use two different approaches to compute the size distribution of the condensates following the phase transition.

In the case that the transition occurs along path ③, we use the homogenous condensation model of Raizer (1960). In this model, when the expanding vapour cloud crosses the vapour–liquid boundary given by the Clausius–Clapeyron equation, the vapour enters first a

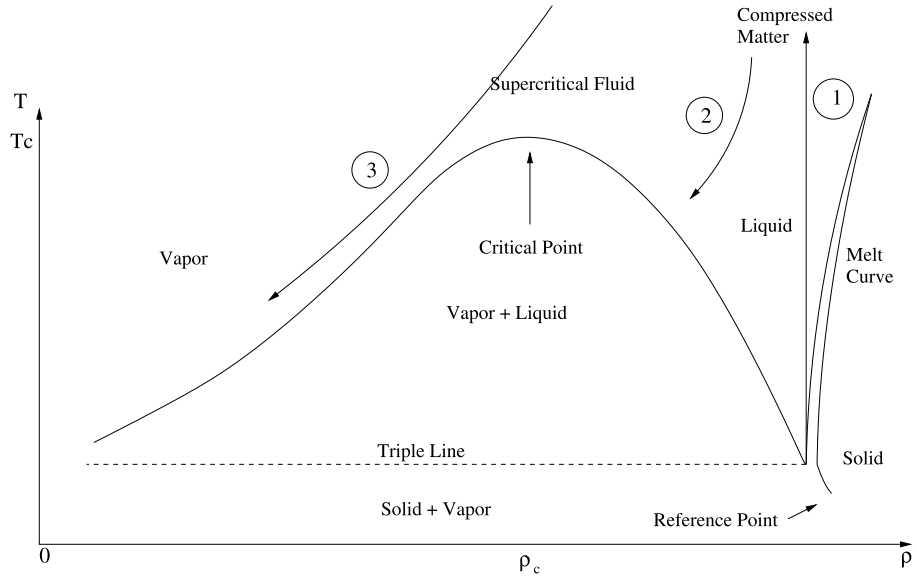


**Fig. 2** Schematic $T$, $\rho$ vapour–liquid–solid diagram. $T_c$ and $\rho_c$ indicate the critical point above which one cannot separate liquid from vapour. The reference point points to room-temperature conditions. The matter is shocked along path ①, and relaxed along the paths ② and ③

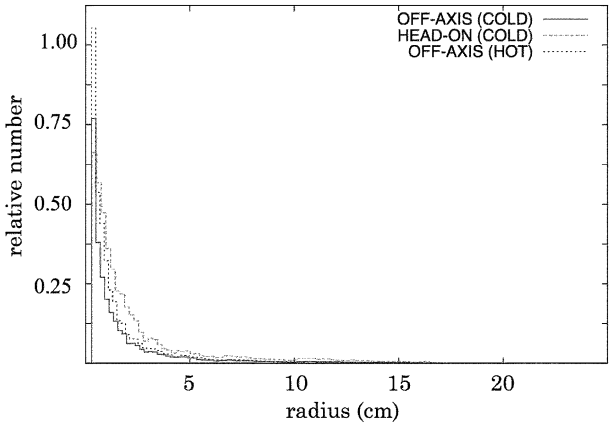


**Fig. 3** Size distribution of particles (condensates and melt droplets) which result from runs 6, 11 and 17 using ANEOS. Particle sizes range from $1.7 \times 10^{-6}$ cm to 22.3 cm for run 6, $1.6 \times 10^{-6}$ cm to 21.4 cm for run 11, and from $1.6 \times 10^{-2}$ cm to 20.7 cm for run 17

saturated and then a supersaturated (metastable) state. The vapour then undergoes a partial transformation into liquid droplets, where each droplet contains some average number of atoms. Their growth is only possible if their volume energy exceeds their surface energy. The number of liquid droplets formed is given by the nucleation rate which depends critically upon the surface tension $\sigma$. In our calculations we adopt $\sigma = 1{,}400$ erg/cm$^2$ for iron (Gail and Sedlmayr 1986) and $\sigma = 350$ erg/cm$^2$ for dunite (Elliot et al. 1963). It is beyond the scope of this paper to discuss this model in more detail, but the interested reader will find more in the original paper and in Anic et al. (2007).

On the other hand, if the hot vapour cools along path ②, we use the formalism provided by Grady (1982) to compute the decompression and fragmentation. We also check whether droplet formation is governed by dynamic fragmentation (Grady 1982) or the liquid to vapour transition (Melosh and Vickery 1991), or both. Here again we refer the reader to the original papers and to Anic et al. (2007) for more details.

The resulting distributions of droplet sizes obtained for runs 4 (head-on, "cold"), 11 (off-axis, "cold") and 17 (off-axis, "hot") are shown in Fig. 3.

For all three runs, the majority of the droplets are less than 5 cm in radius with a peak at or slightly below 1 cm. The differences between the three simulations, as far as the size distribution is concerned, are relatively small. Results obtained using a perfect gas EOS to compute the expansion lead to somewhat smaller condensates. In particular, the peak of the distribution is markedly below 1 cm. We conclude that giant impacts that lead to a suitable fractionation of a chondritic proto-Mercury produce essentially centimeter and subcentimeter sized particles in the ejecta.

### 4.2 Non-gravitational Forces

Several nongravitational mechanisms may perturb the orbit of dust particles. Because we assume that both our proto-Mercury and the impactor are quite large and have differentiated to form iron cores, we may presume that the impact occurs late enough that the nebular gas has dissipated. We may therefore neglect the effect of gas drag on the ejecta; drag due to the modern solar wind is significant only for particles of size less than one micron. Because the overwhelming majority of the condensates and (solidified) melt droplets are less than 1 cm in size, we may also neglect the Yarkovsky effect (see e.g. Bottke et al. 2000). We are left

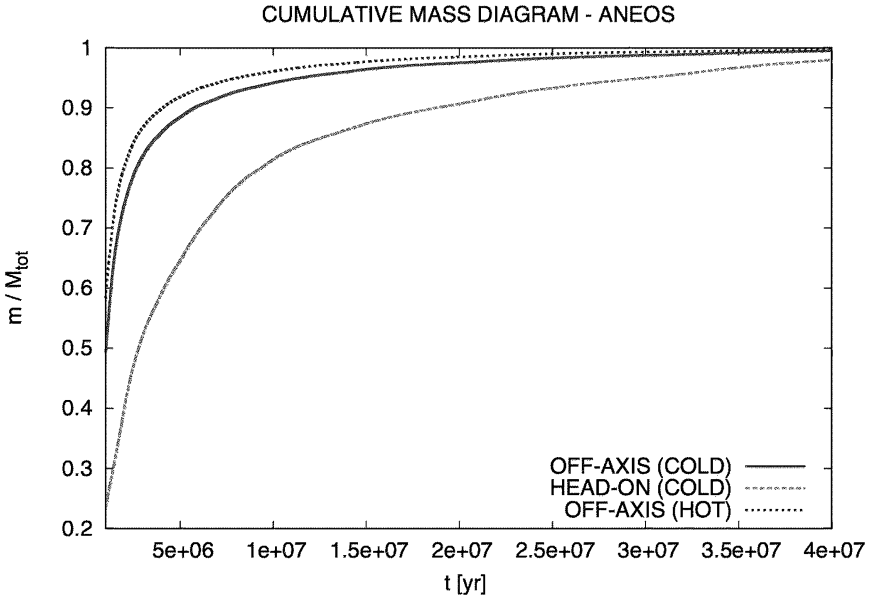


**Fig. 4** The effect of Poynting–Robertson drag on particles with initial orbits and particle sizes determined from our SPH simulations and condensation calculations. Results for three different impact scenarios are shown, and the ANEOS equation of state was used in all cases. The figure shows the mass fraction of ejecta particles collected by the Sun as a function of time after the impact. In the slowest case, for a head-on impact with a cold proto-Mercury, the half-life of the particles is about 2.5 Myr

with direct photon pressure and the Poynting–Robertson effect. For particles of the densities considered here, the Poynting–Robertson effect is dominant for particle sizes greater than 1 micron.

Poynting–Robertson drag arises from the relativistic interaction of dust particles with solar photons. Robertson (1937) investigated the fate of small particles in circular orbits and set up the corresponding equations of motion. Wyatt and Whipple (1950) extended the method to the general case of elliptic orbits. Using the equations published in those papers we can calculate the time scales on which the condensates (and melt droplets) resulting from the simulations presented earlier disappear into the Sun.

Knowing the size distribution of the ejecta and knowing the corresponding material density, we need only the initial orbital elements of the condensates in order to actually compute their removal timescale. We obtain these orbital elements for each ejected SPH pseudo-particle by picking an arbitrary impact site somewhere along proto-Mercury's orbit which gives us the centre of mass velocity to which we add the ejection velocity as computed by the hydrodynamics code. We further assume that all particles are spherical and of uniform density and that they intercept radiation from the Sun over a cross-section $\pi r^2$ and isotropically reemit it at the same rate (thermal equilibrium). The relevant decay equations for this case can be found in Wyatt and Whipple (1950) and Fig. 4 shows the results of applying these equations to the simulated ejecta particles. For simplicity we have neglected the effects of finite size and rotation of the Sun (Mediavilla and Buitrago 1989). The time-scale for removal of particles with our calculated size distribution can be seen to be less than a few million years.

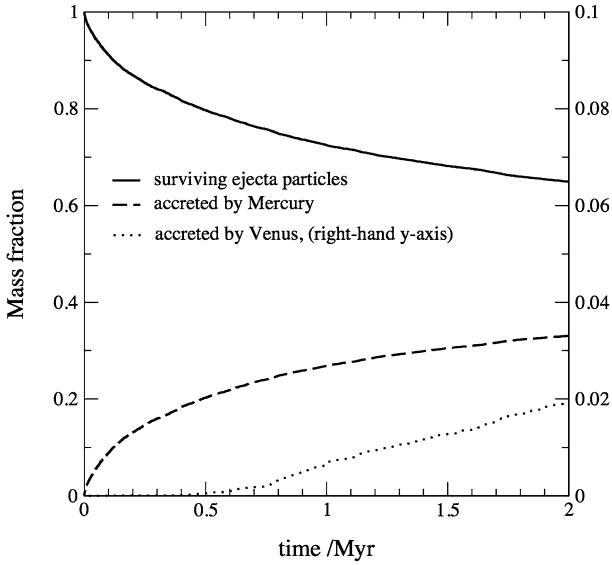


**Fig. 5** Decay of a population of particles ejected from Mercury in a head-on collision (simulation run 6) at the perihelion of the planet's orbit. N.B. the fraction of particles colliding with Venus has been scaled up for better visibility

### 4.3 Collision Time and Gravitational Scattering

The ejecta from the collision initially have heliocentric orbits which still cross the orbit of Mercury. Unless they are removed from such orbits, e.g. by the Poynting–Robertson effect (see Sect. 4.2) or by gravitational scattering, most of the matter will be reaccreted by the planet over time and the resulting collisional fractionation will be too small to explain the planet's anomalous composition.

In order to study the dispersal and reaccretion of the ejected matter under the effects of gravity, a number of simulations were carried using the hybrid integrator MERCURY (Chambers 1999). We simulated the behaviour of a large population of ejected particles under the gravitational influence of Mercury (taken as being the mass of the currently observed planet), Venus, Earth, Mars and Jupiter, for a period of two million years. For lack of a better choice, these planets were placed on their current orbits. The ejected particles were treated as being massless, and were followed until they were either ejected from the inner Solar system (passing beyond the orbit of Jupiter), or collided with one of the planetary bodies. Their initial positions and velocities were computed using hermeocentric velocities chosen randomly from amongst the ejected SPH pseudo-particles, the choice of a position of proto-Mercury on its orbit at the time of the impact and the necessary coordinate transformation from a hermeocentric to a heliocentric frame of reference.

Two different series of integrations were run. The first simulation, which was the most detailed, followed the behaviour of 10,000 ejected particles over the two million year period for the case of a head-on collision. The second series of simulations used a smaller dataset (1,000 particles), but examined the effect of the collision location, the collision geometry (head-on vs. glancing, as described earlier) and the effect of scaling the mass of the remnant planet. Here we show only the results from the simulation involving the large number of particles (Fig. 5). The other simulations yield very similar results except for when the collision occurs at aphelion; in this case the rate of reaccretion is significantly less.

It can clearly be seen from Fig. 5 that the number of surviving particles decays over time, with the bulk of the removed material being lost to reaccretion by Mercury. However, the

rate at which material reaccretes is particularly low—after two million years, 6,496 of the 10,000 particles remain in the simulation, which corresponds to a decay half-life of about 3.2 Myr. Of the 3,504 particles which were removed from the simulation over the course of the 2 million year period, 3,306 were reaccreted by Mercury, while 191 hit Venus, with the remaining 7 particles hitting the Sun or being ejected beyond the orbit of Jupiter. In longer simulations, particles were observed to impact the Earth, and an ever-increasing fraction were ejected from the system rather than being accreted, so it is clear that the particles slowly diffuse throughout the inner Solar system as a result of repeated encounters with the inner planets. These results are consistent with those obtained by Gladman (2003) for slightly different initial conditions. Warrel et al. (2003) found that hermeocentric and 1:1 Mercury mean motion resonance orbits can be stable for long time periods, but that ejecta with velocities only slightly greater than the escape velocity are likely to be reaccreted due to the necessity of successive close encounters with Mercury to achieve significant gravitational scattering. They did not, however, provide a numerical result.

In Sect. 4.2 we showed that the half-life of the condensates is of order 2.5 Myr before they are removed by the Poynting–Robertson effect. Over the same period of time, roughly 40% of particles are found to collide with Mercury. This implies that successful collisions are really those for which the post-collision $R/I$ ratio is somewhat less than Mercury's present-day ratio probably in the range $0.3 \leq R/I \leq 0.4$ in order to allow for this reaccretion. No attempt was made to simulate a collision that would, after reacculation, lead to the exact $R/I$ ratio. However, since our ratios bracket the desired value there would be no problem to find an appropriate collision. We conclude that giant collisions as envisioned here can indeed lead to significant long-term chemical fractionation.

## 5 Summary and Conclusions

We have confirmed, using SPH models with a significantly higher resolution than previous efforts, that a giant impact is capable of removing a large fraction of the silicate mantle from a roughly chondritic proto-Mercury. The size and velocity of the impactor were chosen to be consistent with predictions of planetary formation and growth, and a plausible Mercury can be obtained for several assumptions about initial temperatures and impact parameter.

We extended the previous work on the subject by addressing the fate of the ejecta in order to assess the fraction that could be reaccumulated by Mercury thereby changing again the fractionation achieved immediately after the impact. In particular, using a simple condensation model, we derived the expected size distribution of the ejected material after it cools following adiabatic expansion, and the subsequent dynamical evolution of the resulting particles. The loss of ejected particles into the Sun due to Poynting–Robertson drag was shown to be at least as efficient as reaccretion onto Mercury, and so the bulk density and composition that result from the giant impact would have been largely retained. The giant impact hypothesis for the formation of Mercury is thus entirely plausible.

Our simulations provide estimates of particle size and temperature, and gas density in the ejecta plume. First-order estimates of chemical mixing and loss of volatile elements could perhaps be undertaken with this information. Future simulations will concentrate on chemical fractionation resulting from the impact, and may have sufficient resolution to consider the effect of large ion lithophiles having been preferentially incorporated into a "crust" on the proto-Mercury. These more sophisticated simulations would then be able to make predictions about the isotopic and elemental composition of the modern Mercury. These predictions could then be tested, at least in part, by the data expected from the two coming Mercury spacecraft missions.

Confirming the collisional origin of the anomalous density of Mercury would go a long way toward establishing the current model of planetary formation through collisions which predicts giant impacts to happen during the late stages of planetary accretion. Hence, small Mercury has the potential to become a Rosetta stone for the modern theory of planet formation!

**Acknowledgements** The authors gratefully acknowledge partial support from the Swiss National Science Foundation.

## References

J.D. Anderson, G. Colombo, P.B. Esposito, E.L. Lau, G.B. Trager, Icarus **71**, 337 (1987)
A. Anic, PhD Thesis, University of Bern, 2006
A. Anic, W. Benz, J. Horner, J.A. Whitby, Icarus (2007, in preparation)
A. Balogh, R. Grard, S.C. Solomon, R. Schulz, Y. Langevin, Y. Kasaba, M. Fujimoto, Space Sci. Rev. (2007, this issue). doi:10.1007/s11214-007-9212-4
S.S. Barshay, J.S. Lewis, Annu. Rev. Astron. Astrophys. **14**, 81 (1976)
W. Benz, in *The Numerical Modelling of Nonlinear Stellar Pulsations Problems and Prospects*, ed. by J.R. Buchler (1990), p. 269
W. Benz, A.G.W. Cameron, W.L. Slattery, Icarus **74**, 516 (1988)
W. Benz, A.G.W. Cameron, H.J. Melosh, Icarus **81**, 113 (1989)
W.F. Bottke, D.P. Rubincam, J.A. Burns, Icarus **145**, 301 (2000)
A.G.W. Cameron, Icarus **64**, 285 (1985)
A.G.W. Cameron, B. Fegley, W. Benz, W.L. Slattery, in *Mercury*, ed. by F. Vilas, C. Chapman, M.S. Matthews (University of Arizona Press, Tucson, 1988), 692 pp
J.E. Chambers, Mon. Not. R. Astron. Soc. **304**, 793 (1999)
J.F. Elliot, M. Gleiser, V. Ramakrishna, in *Thermochemistry for Steelmaking*, vol. II (Addison-Wesley, 1963)
B. Fegley Jr., A.G.W. Cameron, Icarus **82**, 207 (1987)
B. Fegley Jr., J.S. Lewis, Icarus **41**, 439 (1980)
H.P. Gail, E. Sedlmayr, Astron. Astrophys. **166**, 225 (1986)
B. Gladman, LPSC **XXXIV**, #1933 (2003)
K.A. Goettel, S.S. Barshay, in *The Origin of the Solar System*, ed. by S. Dermott (Wiley, Chichester, 1978), 611 pp
D.E. Grady, J.A.P. **53**, 322–325 (1982)
H. Harder, G. Schubert, Icarus **151**, 118 (2001)
J.S. Lewis, Earth Planet. Sci. Lett. **15**, 286 (1972)
J.S. Lewis, Science **186**, 440 (1974)
J.S. Lewis, in *Mercury*, ed. by F. Vilas, C. Chapman, M.S. Matthews (University of Arizona Press, Tucson, 1988), p. 651
E. Mediavilla, J. Buitrago, Eur. J. Phys. **10**, 127 (1989)
H.J. Melosh, A.M. Vickery, Nature **350**, 494 (1991)
P. Michel, W. Benz, P. Tanga, D. Richardson, Icarus **160**, 448 (2002)
J.J. Monaghan, Annu. Rev. Astron. Astrophys. **30**, 543 (1992)
J.P. Morris, J.J. Monaghan, J. Comput. Phys. **136**, 41 (1997)
Y.P. Raizer, J. Exp. Theor. Phys. **37**(6), 1229 (1960)
H.P. Robertson, Mon. Not. R. Astron. Soc. **97**, 423 (1937)
E.M. Shoemaker, in *Physics and Astronomy of the Moon*, ed. by Z. Kopal (Academic, New York and London, 1962)
J.V. Smith, Mineral. Mag. **43**, 1 (1979)
T. Spohn, F. Sohl, K. Wieczerkowski, V. Conzelmann, Phys. Space Sci. **49**, 1561 (2001)
A. Sprague, J. Warell, G. Cremonese, Y. Langevin, J. Helbert, P. Wurz, I. Veselovsky, S. Orsini, A. Milillo, Space Sci. Rev. (2007, this issue). doi:10.1007/s11214-007-9221-3
H.S. Thompson, S.L. Lauson, Sandia Labarotories Report SC-RR-710714 (1984)
H.C. Urey, Geochim. Cosmochim. Acta **1**, 209 (1951)
H.C. Urey, *The Planets* (Yale University Press, New Haven, 1952)
J. Warrel, O. Karlsson, E. Skoglov, Astron. Astrophys. **411**, 291 (2003)
S.J. Weidenschilling, Icarus **35**, 99 (1978)
G.W. Wetherill, in *Origin of the Moon*, ed. by W.K. Hartmann, R.J. Phillips, G.J. Taylor (Lunar and Planetary Institute, Houston, 1986), 519 pp
S.P. Wyatt Jr., F.L. Whipple, Astrophys. J. **111**, 134 (1950)

# Mercury's Interior Structure, Rotation, and Tides

**Tim Van Hoolst · Frank Sohl · Igor Holin · Olivier Verhoeven · Véronique Dehant · Tilman Spohn**

Originally published in the journal Space Science Reviews, Volume 132, Nos 2–4.
DOI: 10.1007/s11214-007-9202-6 

**Abstract** This review addresses the deep interior structure of Mercury. Mercury is thought to consist of similar chemical reservoirs (core, mantle, crust) as the other terrestrial planets, but with a relatively much larger core. Constraints on Mercury's composition and internal structure are reviewed, and possible interior models are described. Large advances in our knowledge of Mercury's interior are not only expected from imaging of characteristic surface features but particularly from geodetic observations of the gravity field, the rotation, and the tides of Mercury. The low-degree gravity field of Mercury gives information on the differences of the principal moments of inertia, which are a measure of the mass concentration toward the center of the planet. Mercury's unique rotation presents several clues to the deep interior. From observations of the mean obliquity of Mercury and the low-degree gravity data, the moments of inertia can be obtained, and deviations from the mean rotation speed (librations) offer an exciting possibility to determine the moment of inertia of the mantle. Due to its proximity to the Sun, Mercury has the largest tides of the Solar System planets. Since tides are sensitive to the existence and location of liquid layers, tidal observations are ideally suited to study the physical state and size of the core of Mercury.

**Keywords** Mercury · Interior · Composition · Rotation · Libration · Tides

## 1 Introduction

With a mass of $M = 3.302 \times 10^{23}$ kg and a radius of $R = 2439 \pm 1$ km (Anderson et al. 1987), Mercury is the smallest terrestrial planet and has the second-largest mean density,

T. Van Hoolst (✉) · O. Verhoeven · V. Dehant
Royal Observatory of Belgium, Ringlaan 3, 1180 Brussels, Belgium
e-mail: tim.vanhoolst@oma.be

F. Sohl · T. Spohn
German Aerospace Center (DLR), Institute of Planetary Research, Rutherfordstr. 2, 12489 Berlin, Germany

I. Holin
Space Research Institute, Moscow, Russia

A. Balogh et al. (eds.), *Mercury*. DOI: 10.1007/978-0-387-77539-5_3 

which indicates a large core. If the core consists mainly of iron, the core radius will be about 3/4 of the radius of the planet, resulting in a core-to-mantle size ratio that is larger than for the three other terrestrial planets. If created by a dynamo, the magnetic field observed by Mariner 10 is evidence for a liquid outer core and a strong indication for a solid inner core, which is also predicted by thermal evolution models (Schubert et al. 1988; Hauck et al. 2004; Breuer et al. 2007; Wicht et al. 2007).

The large core implies large differences in bulk composition of Mercury with respect to the other terrestrial planets, and suggests a different formation history (e.g. Benz et al. 2007; Taylor and Scott 2005). A scenario in which Mercury suffered a collision with another large protoplanet is presently the most popular (Taylor and Scott 2005), but other scenarios such as evaporation and condensation models can not be ruled out (for a detailed account of Mercury's formation, see Benz et al. 2007).

Here, we review the present knowledge on Mercury's deep interior and discuss the geodetic measurements that can advance our understanding of Mercury to the level of that of Mars, and even beyond. We do not review the formation, evolution or magnetic field generation in Mercury, although they are obviously and intimately linked to the interior structure and bulk composition, since these topics are treated elsewhere in this issue.

This review is organized as follows. Present constraints on Mercury's composition and internal structure are reviewed in Sect. 2, and possible interior models are described. The large core is probably the property in which Mercury differs most from the other terrestrial planets. In the next sections, we therefore discuss methods that can be used to derive properties of Mercury's core, in particular geodetic methods. The low-degree gravity field of Mercury gives information on the differences of the principal moments of inertia, which are a measure of the mass concentration toward the center of the planet (Sect. 3). These coefficients were determined by radio tracking Mariner 10 during its Mercury flybys in 1974 and 1975, but are too inaccurate for use in the interior structure models. The MESSENGER and BepiColombo mission to Mercury will improve these values to subpercentage level, but even then other geodetic data are needed to obtain the moments of inertia themselves instead of their differences to constrain models of the interior. In Sect. 4, we review the rotational behaviour of Mercury and show that the moments of inertia of the core and the mantle can be determined from observations of the orientation and rotation rate variations (librations), if the degree-two gravity coefficients are known. The gravity information is necessary because the rotation of Mercury depends on the solar gravitational torque on Mercury, whose components are linearly proportional to the degree-two coefficients $J_2$ and $C_{22}$ of the planet's gravity field. With a known gravitational forcing, observations of Mercury's rotation can be used to estimate Mercury's inertia to rotation.

Tides provide another means to obtain insight into the deep interior of Mercury. Tides were already used in the early 20th century to show that the Earth's core is liquid (Jeffreys 1926). Due to its close distance to the Sun, tides on Mercury are larger than those on Earth, and tidal observations are an excellent tool for constraining the constitution of the interior. In Sect. 5, we discuss how constraints on Mercury's interior can be inferred from MESSENGER and BepiColombo tidal measurements. Conclusions are presented in Sect. 6.

## 2 Models of the Interior Structure and Composition

### 2.1 Interior Structure

From the analysis of Mariner 10 Doppler data and radio occultation observations, Mercury's total mass of $3.302 \times 10^{23}$ kg and mean radius of $2439 \pm 1$ km was inferred. The determi-

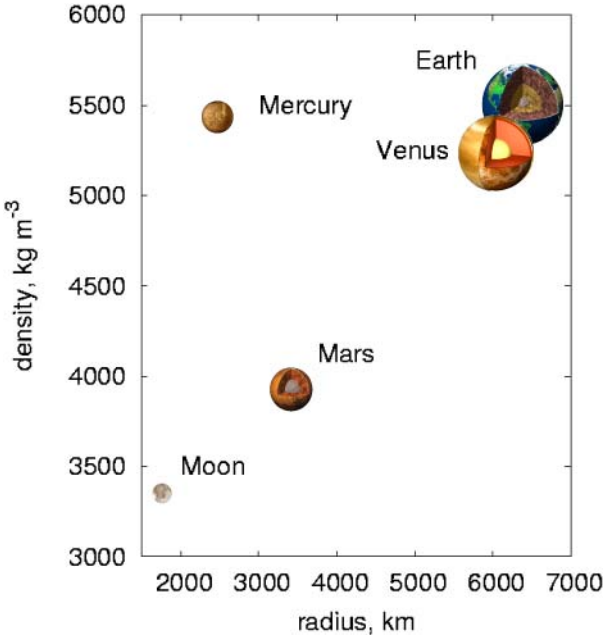


**Fig. 1** Radius–density relation of the terrestrial planets and the Moon. Note the anomalous mean density of Mercury that implies an iron-rich interior and peculiar formation history of the planet

nations of the planet's mass and radius resulted in a mean density of $5430 \pm 10\ \mathrm{kg\,m^{-3}}$ (Anderson et al. 1987), which is comparable to that of the Earth and Venus but much larger than those of the Moon and Mars (Fig. 1). Though substantially smaller in size, Mercury's surface gravity of $3.7\ \mathrm{m\,s^{-2}}$ almost equals that of the larger planet Mars.

If extrapolated to zero-pressure, Mercury's density is about $5300\ \mathrm{kg\,m^{-3}}$, i.e., much higher than the uncompressed densities of Earth, Venus, and Mars which are about 4100, 4000 and $3800\ \mathrm{kg\,m^{-3}}$, respectively. This suggests that Mercury contains a much larger proportion of heavier elements than any other terrestrial planet. The relative abundance of iron could for example be about twice that of the Earth (Wasson 1988). The existence of the weak intrinsic magnetic field and compressional surface features observed by Mariner 10 together with the large average density suggest that most of the iron is concentrated in a partially liquid iron-rich core with a radius of roughly 0.8 times the total radius of Mercury. The core occupies about half of the planet's volume corresponding to a core mass fraction of 2/3 relative to the planet's mass or about twice that of the Earth (Siegfried and Solomon 1974).

If Mercury were in hydrostatic equilibrium, its moment of inertia could be determined from the observed flattening as an additional constraint on the interior structure. The degree-two coefficients $J_2$ and $C_{22}$ of the gravity field of Mercury were determined from Doppler and range data on the radio link between Mariner 10 and Earth during the first and third encounter of the spacecraft with Mercury in March 1974 and March 1975. A reanalysis by Anderson et al. (1987) resulted in $J_2 = (6 \pm 2) \times 10^{-5}$ and $C_{22} = (1.0 \pm 0.5) \times 10^{-5}$. The polar flattening caused by rotation would give a $J_2$-value two orders of magnitude smaller, indicating that $J_2$ is mainly due to nonhydrostatic effects. These effects are also larger than for the other slowly rotating planet Venus, which has $J_2 = (4.404 \pm 0.002) \times 10^{-6}$ and $C_{22} = (1.57 \pm 0.02) \times 10^{-6}$ (Konopliv et al. 1999). Moreover, ground-based radar ranging data suggest that the equatorial shape of Mercury is significantly elliptical (Anderson et al. 1996). These observations show that Mercury has not attained an equilibrium figure. There-

fore, its shape and gravitational field cannot be used to infer the size of its metallic core. From a comparison between the equatorial shape and the gravitational equatorial ellipticity $C_{22}$, Anderson et al. (1996) have concluded that the crust could be $200 \pm 100$ km thick if Mercury's equatorial ellipticity were entirely compensated by Airy isostasy. The crust thickness has also been estimated from constraints on the heat flow into the base of the crust from observations of ancient faults (Nimmo 2002). Taking into account that the base of the crust does not melt, Nimmo and Watters (2004) derived an upper bound on the crustal thickness of 140 km. The large crust thicknesses deduced from Mercury's shape and surface tectonics are difficult to reconcile with the planet's magmatic evolution.

Models of the interior structure rely on the mass and mean radius of the planet since a value for the moment-of-inertia (MoI) factor is not available at present. A determination of the MoI factor, as envisioned by future missions to Mercury, would help distinguish an iron core from a more homogeneous distribution of iron in oxidized form within the planet (Schubert et al. 1988). The spectral characteristics and high albedo of the surface of Mercury are consistent with the existence of a metal-poor and possibly highly differentiated, feldspathic crust that contains less FeO and $TiO_2$ than the lunar highland crust. This is taken as evidence for the strong internal differentiation of the planet (Jeanloz et al. 1995; Sprague et al. 2007).

To construct depth-dependent models of the interior structure of Mercury, a spherically symmetric planet in perfect mechanical and thermal equilibrium is assumed. The following set of differential equations for mass $m$, iron mass $m_{Fe}$, mean moment of inertia $\theta$, acceleration of gravity $g$, pressure $p$, and heat flux $q$ can be derived from fundamental principles (Sohl and Spohn 1997):

$$\frac{dm}{dr} = 4\pi r^2 \rho, \tag{1}$$

$$\frac{dm_{Fe}}{dr} = x_{\mathrm{Fe}} \frac{dm}{dr}, \tag{2}$$

$$\frac{d\theta}{dr} = \frac{8}{3}\pi r^4 \rho, \tag{3}$$

$$\frac{dg}{dr} = 4\pi \mathrm{G}\rho - 2\frac{g}{r}, \tag{4}$$

$$\frac{dp}{dr} = -\rho g, \tag{5}$$

$$\frac{dq}{dr} = \rho\epsilon - 2\frac{q}{r}, \tag{6}$$

where $r$ is the radial distance from the center of the planet, $G$ the gravitational constant, $\rho$ the density, $x_{\mathrm{Fe}}$ the concentration of iron per unit mass, and $\epsilon$ the specific heat production rate.

Heat is primarily carried by conduction across the stagnant outer portion of Mercury's silicate shell and the top and bottom thermal boundary layers of mantle convection (Breuer et al. 2007). The corresponding radial temperature gradient is given by

$$\frac{dT}{dr} = -\frac{q}{k}, \tag{7}$$

where $k$ is the thermal conductivity. Within the convective portion of the silicate shell and the liquid outer core, the temperature gradient can be approximated by the adiabatic temperature

gradient (Stacey 1977)

$$\frac{dT}{dr} = T\frac{\gamma}{K_S}\frac{dp}{dr}, \tag{8}$$

where $\gamma = \alpha K_S/\rho c_p$ is the thermodynamic Grüneisen parameter, $c_p$ the specific heat, $\alpha$ the thermal expansion coefficient, and $K_S$ the adiabatic bulk modulus.

The set of basic differential equations (1–8) can be separated into two subsets that are coupled through the density $\rho$. The mechanical properties of the interior are calculated from (1–5), while (6–8) give the thermal structure of the model. These equations have to be supplemented with equations of state to include pressure-induced compression and thermal expansion effects on the density. For example, a third-order isothermal Birch–Murnaghan can be used to correct for the pressure-induced compression, and temperature corrections can be done through the use of a thermal-pressure term, according to

$$p = \frac{3K_{0T}}{2}\left[\left(\frac{\rho}{\rho_0}\right)^{7/3} - \left(\frac{\rho}{\rho_0}\right)^{5/3}\right]\left\{1 + \frac{3}{4}(K_0' - 4)\left[\left(\frac{\rho}{\rho_0}\right)^{2/3} - 1\right]\right\} + \alpha_0 K_{0T}\,(T - 298) \tag{9}$$

(Baumgardner and Anderson 1981). Here, $K_T$ is the isothermal bulk modulus, $K'$ its derivative with respect to pressure, and subscripts zero denote standard pressure and temperature conditions at $p = 0$, $T = 298$ K. Additional assumptions about the chemistry and densities of a basaltic crust, a more primitive mantle, and an iron-rich core are then required to construct models of the interior in accordance with the mass and mean density of the planet (Wood et al. 1981).

## 2.2 Composition

Mercury is the only terrestrial planet other than the Earth with a perceptible dipole magnetic field. The presence of an internally-generated magnetic field suggests that the iron core is at least partially liquid with an electrically conducting outer core of unknown thickness surrounding a solid inner core. Thermal evolution models indicate that the core would have solidified early in the history of Mercury unless a light alloying element such as sulfur were present (Breuer et al. 2007). A small amount of sulfur as suggested by Stevenson et al. (1983) is sufficient to depress the freezing point of the core alloy and is consistent with the refractory bulk composition Mercury should have acquired if it accreted in the hot innermost part of the solar nebula.

Most studies assume the core to be composed of iron (Fe) and sulfur (S), but other light elements (O, H, ...) and heavy (Ni) elements could also be present (although the lower pressures strongly reduce the solubility of, e.g., oxygen compared to the Earth). Sulfur has the important property that it lowers the melting temperature with respect to that of pure iron, contrary to oxygen, for example (Williams and Jeanloz 1990). The concentration of sulfur is unknown and depends critically on the origin of Mercury, in particular where the planetesimals from which the planet formed came from (Wetherill 1988). If Mercury formed close to its present position, its sulfur concentration would probably be very low (Lewis 1988). However, if Mercury formed in the same feeding zones as Earth, Venus, and Mars, its light element concentration could be higher and closer to that of those planets. The Earth's core has a light-element concentration of about 10 wt% (Poirier 1994), and for Mars, a sulfur concentration of 14 wt% in the core is often considered (Longhi et al. 1992), although smaller values even down to 0.4 wt% (Gaetani and Grove 1997) have been obtained.

As a consequence of the planet's cooling history, a solid inner core surrounded by a volatile-rich liquid outer core may have formed on Mercury. Inner-core growth by solid-iron precipitation occurs when the local core temperature drops below the local liquidus temperature. At the low core pressures in Mercury, sulfur strongly partitions in the liquid, and the inner core is expected to be composed of almost pure iron, if the initial sulfur concentration at formation was less than the eutectic concentration (Li et al. 2001). Therefore, the liquid outer core will gradually increase its light element concentration until it attains the eutectic composition, which is characterized by a sharp minimum in the liquidus curve. Upon further cooling, the outer core liquid gradually freezes, and solids of eutectic composition are deposited onto the solid inner core. In such an evolution stage, compositional buoyancy is absent in the outer fluid core, and it seems unlikely that a dynamo generating a global magnetic field can be effective. The magnetic field observation then suggests that Mercury's inner core radius should be smaller than that at which the core fluid becomes eutectic (see, e.g., Christensen 2006; for a detailed description in this issue, see Breuer et al. 2007 and Wicht et al. 2007).

Thermal history models taking into account parameterized convective heat transport through the mantle indicate sulfur concentrations of 1 to 5% to retain a liquid outer core at the present time (Stevenson et al. 1983; Schubert et al. 1988; Spohn 1991). More sophisticated models of mantle convection including pressure and temperature-dependent rheology demonstrate that the cooling history of a terrestrial planet is governed by the growth of its lithosphere while the deep interior remains relatively hot. These models compare well to the parameterized convection calculations but produce thicker outer core at identical sulfur concentrations. Depending on the stiffness of the mantle rheology, a liquid outer core is then sustained even for sulfur concentrations as small as 0.2% consistent with cosmochemical arguments in favor of a volatile-poor planet (Conzelmann and Spohn 1999; Spohn et al. 2001).

At the typical pressures and temperatures of Mercury's core, solid iron is in the fcc phase ($\gamma$ iron, Anderson 2002), and FeS in the high-pressure phases FeS IV and FeS V (Fei et al. 1995). Moreover, at pressures between 14 GPa and 18 GPa, an intermediate iron-sulfide compound $Fe_3S_2$ forms (Fei et al. 1997), and, at a pressure of 21 GPa, two new additional compounds, $Fe_3S$ and $Fe_2S$, were obtained by Fei et al. (2000). Density values for solid fcc iron and FeS IV are $\rho_{Fe} = 8094\ \mathrm{kg\,m^{-3}}$ (Sohl and Spohn 1997) at standard conditions, i.e., atmospheric pressure and 25°C, and $\rho_{FeS} = 4940\ \mathrm{kg\,m^{-3}}$ at zero pressure and 800 K (Fei et al. 1995). In the liquid state, the density values are somewhat smaller, but the density difference is not well known (e.g., Hixson et al. 1990; Sanloup et al. 2002). An estimate of the density difference of iron of 3.5% at core conditions, derived from data for density changes associated with phase transitions of pure iron at triple points, has been used in Mercury models by Van Hoolst and Jacobs (2003). Most often, the difference in densities between liquid and solid phases is neglected in planetary models (e.g., Harder and Schubert 2001), or relatively small values around 1% are taken, which are typical for $\epsilon$-iron at the Earth's inner core boundary (Boehler 1996). However, in the Earth's core, iron is in the hcp phase ($\epsilon$-iron) instead of the fcc phase ($\gamma$-iron), and the pressure is more then 10 times larger, about 330 GPa at the inner core boundary.

From measurements of lobate scarps on Mercury's surface, Strom et al. (1975) deduced that the radial contraction of Mercury after the heavy bombardment period is limited to about 2 km. This 2 km radial contraction of Mercury in the absence of large-scale magmatism about 4 Gyr ago may be linked to core shrinking due to solid inner core growth and mantle cooling governed by lithospheric thickening and sluggish mantle convection (Schubert et al.

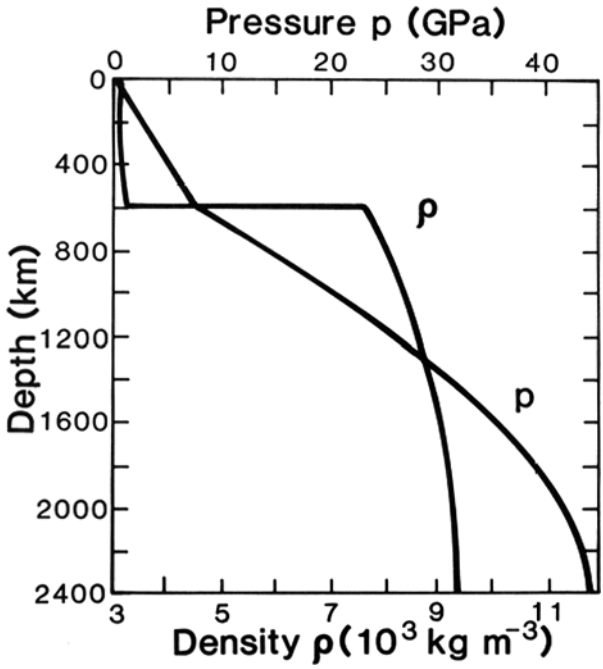


**Fig. 2** Variation of pressure $P$ and density $\rho$ versus depth for a fully differentiated model of Mercury's interior. Note that a refractory bulk composition is assumed. (From Schubert et al. 1988, after Siegfried and Solomon 1974)

1988; Breuer et al. 2007). The density increase upon core solidification is a crucial parameter in the study of this effect, but is, unfortunately, not well known.

The mantle composition of Mercury is uncertain for lack of relevant observational data. Nevertheless, an estimate of the iron content of the mantle has been derived from Earth-based observations. Spectroscopic studies show that the surface of Mercury has a FeO content $\lesssim 3$ wt% (Sprague et al. 1994; Jeanloz et al. 1995). Since many smooth plains with low FeO content have morphological features consistent with a lava flow origin and the FeO content of lava is considered to be close to that of the mantle source region, Robinson and Taylor (2001) concluded that Mercury's mantle is equally low in FeO. Models for the bulk composition of the silicate shell have been proposed that satisfy this constraint and depend on the formation scenario of Mercury (see Taylor and Scott 2005). Mercury's mantle, like the mantle of Mars and the upper mantle of the Earth, essentially consists of olivine, pyroxene, and garnet, with relative proportions strongly dependent on the compositional model. Density discontinuities induced by major phase transitions should not be present in the mantle due to the small pressure increase with depth resulting in a pressure at the core-mantle boundary of at most about 8 GPa (Siegfried and Solomon 1974; Harder and Schubert 2001). It cannot be safely excluded, however, that compositional changes occur across the silicate mantle.

Model calculations show that the moment of inertia factor ranges from 0.325 for fully differentiated models with low sulfur content in the core and low mantle density to 0.394 for chemically homogeneous, undifferentiated models (see Fig. 2). The silicate shell comprising crust and mantle layers is at most 700 km thick, for a pure iron core and large mantle density (Siegfried and Solomon 1974; Harder and Schubert 2001; Spohn et al. 2001). The inner core radius of Mercury can vary between zero and the total core radius, but magnetic observations suggest an inner core to be present and smaller than that for an eutectic outer core. For low sulfur concentration in the core, this maximum core size is close to the total core size (Spohn